Electrochemical Studies of Microwave Synthesised Bimetallic Sulfides Nanostructures As Faradaic Electrodes

A. Bello[a*], O. O Fashedemi[b], D. Y. Momodu[a] F. Barzegar[a], T. M. Masikhwa[a], M. J. Madito[a], F. Taghizadeh[a], J. K. Dangbegnon[a] and N. Manyala[a*]

[a]Department of Physics, Institute of Applied Materials, SARCHI Chair in Carbon Technology and Materials, University of Pretoria, Pretoria 0028, South Africa.

[b]Department of Chemistry, University of Pretoria, Pretoria 0002, South Africa.

***Email address**: ncholu.manyala@up.ac.za (N. Manyala) and bellohakeem@gmail.com (A. Bello)

Corresponding author Tel: +27 (0)12 420 3549, Fax: +27 (0)12 420 2516

Abstract

A microwave irradiation method has been used to prepare mixed nickel cobalt sulfide ($Ni_xCo_yS_4$) nanosheets with different stoichiometric composition as electrodes for electrochemical capacitors. This study has been undertaken to determine the effect of synthesis time and concentration of nickel on the morphology and pseudocapacitance behavior of the $Ni_xCo_yS_4$. It was observed that the time had an effect on the morphology of $Ni_xCo_yS_4$, producing sheet-like (leaf-like) morphology which curls in flower-like shapes with increase in growth (synthesis) time. The effect of morphology on the electrochemical behavior was studied by cyclic voltammetry (CV), chronopotentiometry (CP) and electrochemical impedance spectroscopy (EIS) techniques in aqueous solutions. The sample with a concentration ratio of 2:1 of nickel and cobalt ($Ni_xCo_yS_{4-3}$) shows higher faradaic performance when compared to other samples grown under similar conditions but with different ratios. The maximum specific capacitance values obtained for was 1110 F g^{-1} at a

scan rate of 5 mV s^{-1} for this sample. The Coulombic efficiency of the sample was ~ 80 % after 2000 galvanostatic charge-discharge cycles at a current density of 5 A g^{-1}.

KEYWORDS: Microwave technique, binary metal oxides, sheet-like structure, faradaic electrodes, and electrochemical properties.

INTRODUCTION

The increasing consumption of the fossils fuel with related carbon emissions, the complex set of issues associated with the generation and use of electricity has raised an urgent need and demand for reliable, renewable and sustainable energy alternatives [1,2]. Electrochemical energy-storage systems such as batteries and supercapacitors show considerable promise. Supercapacitors have emerged as a fast-rising class of energy storage technology and have received tremendous attention for potential applications in high-power sources such as portable electronics devices, heavy transport, memory backup system and electric vehicles because of their significant properties which includes: high power density, long cycle life, rapid charge time and safe operation mode [1,3].

Nanostructured materials are being considered as more suitable electrode materials due to their large specific surface area. This is because the performance of the supercapacitor device fabricated will depend on the properties of the applied materials. Generally, large surface area and smaller particle size are beneficial because they provide numerous electroactive sites for adsorption or accommodation of ion from the electrolyte during electrochemical process and can also shorten the ion and electron-transport pathways, thus providing good mechanical and structural stability to reach long cycling, hence improving the performance of the device [4].

As a result of this, Nanostructured transition metal oxides (TMOs) have attracted extensive and intensive research attention in the past few years as pseudocapacitive electrode materials to develop energy-storage devices. TMOs such as RuO_2, MnO_2, Co_3O_4, $Ni(OH)_2$, MoO_3, V_2O_5, NiO etc. have all been explored as pseudocapacitive electrode materials [5–11]. Nevertheless, the low electron conductivity of transition metal oxides, the intrinsically low surface area and non-porosity of the TMOs leads to inferior rate capability and relatively poor electrochemical performance which has largely limited their commercialization [12].

To address this issue and improved on the electrochemical performance, mixed metal oxides, transition metal sulfides including both binary and ternary materials with stoichiometric composition have recently been investigated as novel pseudocapacitive materials for supercapacitors due to their outstanding electrochemical properties, rich redox reactions involving different ions, complex chemical compositions and their synergetic effects [13–17]. Compared to single and simple metal oxides, mixed metal oxides or sulfides exhibit variable oxidation state, high electrical conductivity due to lower activation energy for electron transfer between cations [18–20]. Among the different nanostructured mixed metal oxides, $Ni_xCo_yS_4$ is considered as a promising electrode material because of its low-cost, environmentally benign nature, good electronic conductivity, high theoretical capacitance and rich electrochemical activity (redox reaction) [21]. $Ni_xCo_yS_4$ can be synthesized using different techniques resulting in diverse structural morphologies such as nanoplatelets, [22] nanoprisms [23], nanotubes [24] and microspheres [25].

The development of different ternary nickel cobalt sulfides with controllable composition by different synthesis technique has been documented. Most of the techniques in the literature are mainly based on electrochemical co-deposition and hydrothermal

decomposition of the precursor salts in autoclave systems leading to different morphologies [26]. Recently, Lou *et. al*. prepared hollow $Ni_xCo_{3-x}S_4$ nanoprisms that were sulfurized from a Ni-Co precursor and the hollow prisms exhibited a specific capacitance of 895.2 F g^{-1} at a current density of 1 A g^{-1} in the three-electrode configuration [23]. Similarly, urchin-like nanostructures of $NiCo_2S_4$ were prepared by Xia *et. al.* the urchin-like nanostructures demonstrated a high capacitance of 1149 F g^{-1} at current density of 0.5 A g^{-1} in the three-electrode configuration [25]. Studies of porous nickel cobalt sulfides with different stoichiometry by Haichao Chen suggested that the 1:1 concentration of Ni :Co gave the best electrochemical results for the sulphides they produced [27]. However, as stated earlier most of the reports make use of conventional autoclave technique takes considerable long period of time (12-24 hours) to produce the required materials with desired morphologies. Hence an alternative route which is relatively faster and maintains the capacitive nature of target material at the same time should be explored for the production of the $Ni_xCo_yS_4$ ternary nano composites. In this article, we have used the microwave irradiation technology to produce nano sheet-like structure of nickel, cobalt and sulfides of different ratio by tuning the stoichiometric composition. The advantage of the microwave technology over conventional techniques is that it has rapid kinetics of crystallization therefore reducing reaction times and increase productivity of materials when compared to other conventional available techniques. The as-prepared $Ni_xCo_yS_4$ presents good capacitance values, good rate capability and cycle stability making them promising potential electroactive electrode materials for Faradaic applications.

2. EXPERIMENTAL SECTION

2.1. Materials synthesis.

All the chemicals used were of analytical grade which are commercially available and were used as received. Deionized water was used during all the experimental processes. Ni-Co-S with different composition was prepared using microwave technique. 4 mM $Co(NO_3)_2$ $6H_2O$, 0.8 M thiourea ($CS(NH_2)_2$), with varying concentrations of $Ni(NO_3)_2$ $6H_2O$ (4, 6, 8, and 10 mM) and 2 M of a buffer solution of hexamethyltetraamine ($C_6H_4N_4$) were added to a mixed solvent of water and ethylene glycol (3:1) after which the mixture was stirred for 10 minutes to ensure a homogeneous solution of all the precursors. The resulting transparent solution was then transferred into a quartz vessel in a microwave reactor (Anton Paar Synthos 3000 multimode reactor, 1400 W magnetron power) equipped with a wireless pressure and temperature sensor. The reactor was operated in the pressure mode using a power of 450 W; the sample temperature was ramped at 10 °C/minutes to 120 °C and kept constant at this temperature for different reaction times of 30, 60 and 90 minutes, while the pressure was maintained at 80 bars throughout the hold period. After cooling the reaction chamber to room temperature, the resulting solid precipitates of Ni–Co-S were collected and washed with deionized water and ethanol several times. The samples were then dried at 60 °C for 24 h. The obtained Ni-Co-S samples were designated as Ni-Co-S-1, Ni-Co-S-2, Ni-Co-S-3, and Ni-Co-S-4 respectively, where 1-4 represents the various concentration of the Ni precursor. For example, Ni-Co-S-1 is the sample with 4 mM of $Ni(NO_3)_2$ $6H_2O$ while Ni-Co-S-4 represents the sample grown with 10 mM of $Ni(NO_3)_2$ $6H_2O$. The reaction time was varied from 30-180 minutes in order to determine the optimum time for the best stoichiometric composition.

2.2. Material characterization

Powder X-ray diffraction (XRD) was recorded in the 2θ range between 20.0–80.0 using an XPERT-PRO diffractometer (PANalytical BV, the Netherlands) with theta/2theta geometry and a counting time of 15.240 seconds per step. Qualitative phase analysis of samples was conducted with the X'pert Highscore search match software at room temperature using Co K1α (ʎ=0.178897 nm). The energy dispersive x-ray (EDX) was used to determine elemental composition using scanning electron microscope (SEM) (JEOL 5800LV) equipped with energy dispersive operated at 20 kV, while the morphology and microstructure of the samples were characterized by the high resolution Zeiss Ultra plus 55Field emission scanning electron microscope (FE-SEM) operated at 2.0 kV. The specific surface area and the porosity distributions were calculated from nitrogen adsorption/desorption isotherms and the Barrett–Joyner–Halenda (BJH) method, respectively using Micromeritics TriStar II 3020 (version 2.00) analyzer at 77 K, the samples were outgassed for 12 hours at 90 °C before measurements were taken. The magnetic properties of our samples were carried using SQUID – type magnetometer from Quantum Design (San Diago).

2.3 Electrochemical testing

All the electrochemical tests were conducted under ambient temperature using a beaker-type three electrode system with Ni-Co-Si samples as working electrodes, a glassy carbon plate as a counter electrode and a Ag/AgCl reference electrode in 6 M KOH aqueous electrolyte media. The working electrode for evaluating the electrochemical properties of nickel cobalt sulfides (Ni-Co-S) samples were fabricated by mixing 80 wt.% of Ni-Co-S sample with 10 wt.% carbon black and 10 wt.% of polyvinylidenedifluoride (PVdF) binder in an agate mortar. Few drops of 1-methyle 2-pyrrolydone (NMP) was added to form a paste. The paste

was then coated on a nickel foam current collector (0.2 mm thick) with a coating area of (1 x1 cm^2), pressed at 10 MPa and dried at 60 °C for 8 h in an electric oven to ensure complete evaporation of the NMP. The approximate mass loading of the electroactive materials in each electrode was between 15-20 mg. Cyclic voltammetry (CV), chronopotentiometry (CP) and electrochemical impedance spectroscopy (EIS) studies were performed using a Bio-logic SP-300 potentiostat. The CV tests were carried out in the potential range of 0 to 0.5 V at different scan rates ranging from 5 mV s^{-1} to 100 mV s^{-1}. The CP measurements were also carried out at different current densities: from 1 A g^{-1} to 10 A g^{-1} and the EIS studies were carried out in the frequency range of 100 kHz- 0.01 Hz with 0 V AC amplitude. The gravimetric specific capacitance in (F g^{-1}) was calculated from the CV and CD curves according to equations 1and 2 below:

$$C_{sp} = I\Delta t/\Delta Vm \quad (1)$$

$$C_{sp} = \frac{\bar{A}}{m\Delta V\bar{f}} \quad (2)$$

where, I refers to the discharge current, Δt represents the discharge time; ΔV denotes the voltage interval and m is the mass of the coated active material (in g); $\bar{A}$ is the integrated area under the curve for the cathodic current of the CV curve (in mA-V); and f is the scan rate (in mV/s) used during the CV measurement

Results and discussion

The X-ray diffraction patterns of sample prepared for all the reaction periods are shown in Figure 1 (a-c). The XRD results show representative peaks that can be indexed to the (220), (311), (400), (331), (400), (533), and (551) which crystallizes into the crystal planes of the

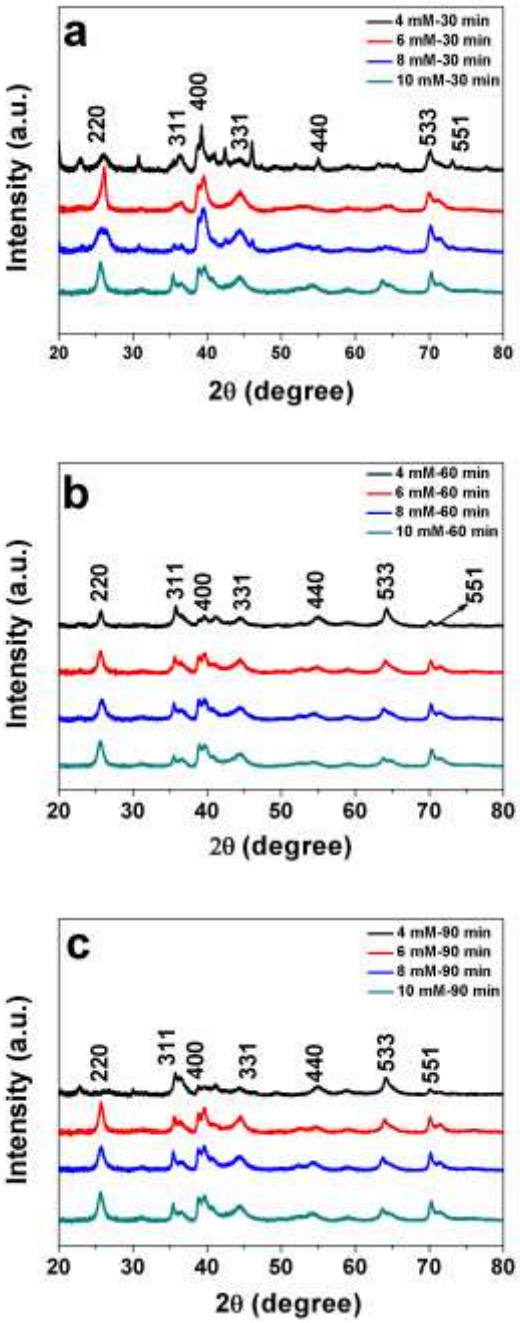

Figure 1 XRD pattern of Ni-Co-S powder with various concentrations at (a) 30, (b) 60 and (c) 90 minutes reaction time respectively.

cubic $NiCo_2S_4$ phase (COD: 96-900-9853 or JCPDS No. 43–1477) [25] with space group Fd-3m(227) and lattice parameter a= 9.4240 Å. These peaks appear for all the samples produced with different concentrations and growth times. The XRD reveals the phase purity and cubic crystalline structure of the as-produced Ni-Co-S powders. The well-defined peaks

are indication of the purity and crystallinity of the sample. Generally, Figure 1 (a) shows a more intense (220), (311), (400) and (331) peaks in comparison to those of Figures 1 (b) and (c), hinting at a more crystalline materials. This may be attributed to the greater presence of unreacted nickel salt as a result of the shorter synthesis time. The XRD patterns in Figures 1 (b) and 1 (c) do not seem to display any differences; with both exhibiting broader and smaller peaks. The (220) peak was used to estimate the grain sizes of each sample using the Scherrer equation assuming spherical shape. From this equation the grain sizes for the samples produced varied with increasing Ni^{+} concentration between ~22.4-25 nm for 30 minutes, ~18-25 nm for 60 minutes and ~16.4-25 nm for 90 minutes.

Figures S1 (a-c) in the supporting information show some representative EDX patterns which provide semi quantitative information on the elemental composition of the as synthesized samples of Ni:Co:S (Co: Ni; 4:6) at the three different synthesis times. The elemental ratio of Ni:Co:S varied according to the concentration of the Ni-precursor. For example typical atomic percent data gave: Co 14.6 ±0.5% and Ni 26.8±0.6% (a); Co 15.9 ±0.6% and Ni 25.0±1.0% (b) and Co 16.9 ±0.5% and Ni 23.0±0.7% (c) This already indicates the facile formation of Ni-Co-S using the microwave technique. Also, one readily observes the representative peaks of the elements present in the composites, showing that the samples produced constituted mainly of Ni-Co-S with negligible trace of impurities; the purity of the samples are in agreement with the XRD results.

The SEM micrographs of the Ni-Co-S with varying concentrations of Ni^{+} and growth times are shown in figure 2. The reaction time was varied to study the effect of time on the various concentrations of the Ni-Co-S samples produced. Irrespective of the different Ni and Co molar ratios the produced sulfides show similar pattern in the morphology and structural

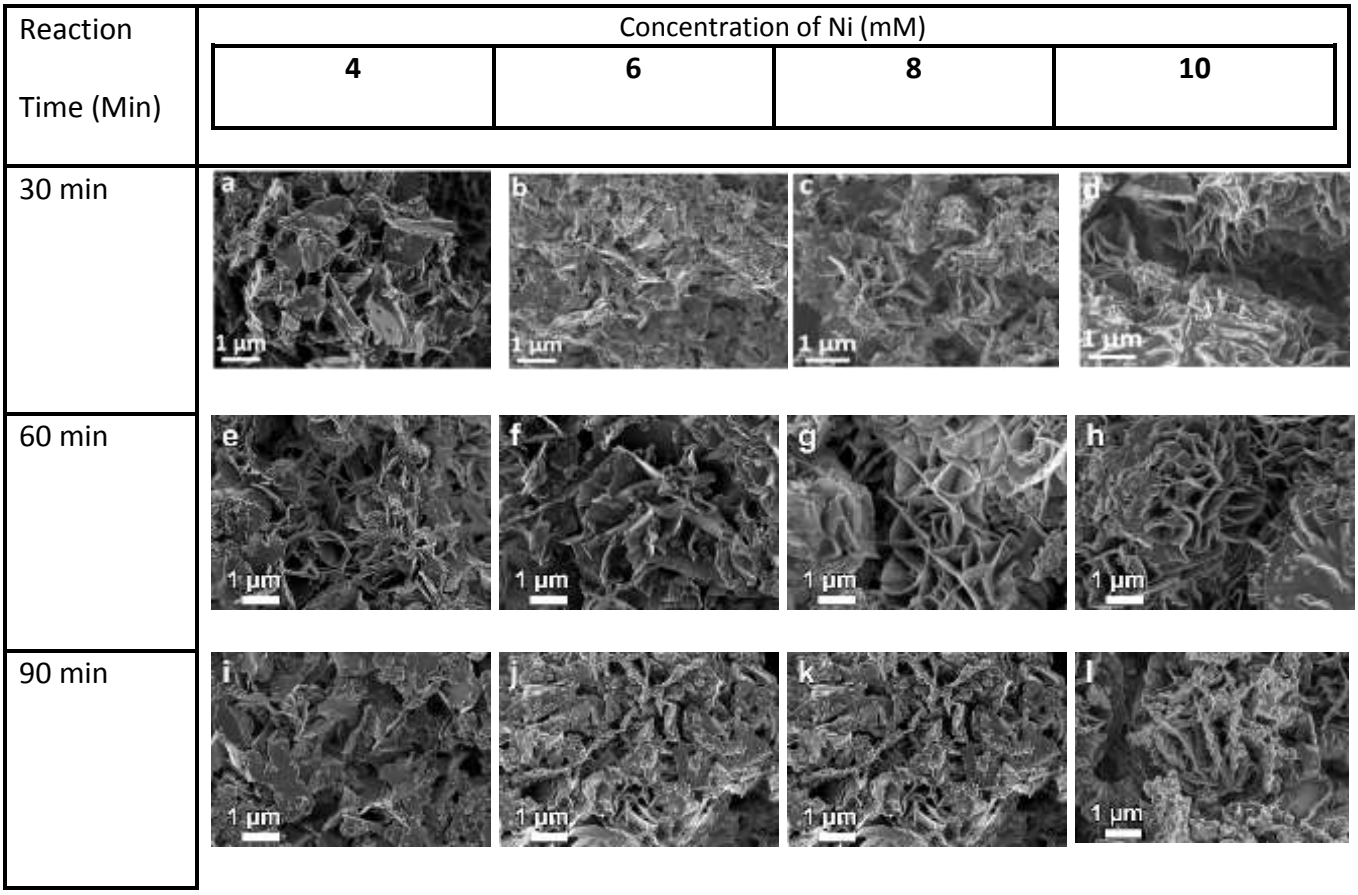

Figure (2) SEM micrographs of Ni-Co-S produced at different times: 30 (a-d), 60 (e-h) and 90 (i-l) minutes with the varying concentration of the Ni precursor.

evolution for each set of samples. Initial set of samples produced for 30 minutes had "cactus-leaf" like (sheets are wider and longer) structures. When the molar concentration of Ni^{+} was increased there seems to be no obvious change in the morphology, rather the "cactus leaf like" morphology loses its definite shape and now appears more crumpled. Further increase in the reaction time to 60 minutes leads to curling and/or wrapping of the nano leaves into flower shape formation. The wrapping is more intense with increase in Ni^{+} concentration. However, for the samples with 90 minutes reaction time; the morphology trend appears to be from the appearance of folded or rumpled leaf-like structures to better defined shapes but not exhibiting a perfect flower morphology, as concentration of Ni^{+} increases. In addition, for all the samples studied there is a steady increase of the diameters

of the nano leaves from a few nanometres, to hundreds of micro-meters when the time was increased from 30 to 90 minutes. The formation mechanism of the leaves which evolves to flower like structures could be explained as follows: Microwave irradiation is based on efficient interaction of molecules with the electromagnetic waves, the electromagnetic waves couple directly with the molecules of reactant in the entire reaction vessel. This leads to a rapid rise in temperature and formation of large amount of nuclei in a short time which is followed by self-assembly of nanoparticles. Since this process is not limited by the thermal conductivity, Ostwald ripening process could also occur. In brief smaller particles dissociates while the bigger ones grow into layers with a lamellar structure, these leaf-like particles tend to curl and assemble forming the flower-like structure [28]. When the time was increased to 90 minutes the flower-like structure expected did not attain a complete growth; this could be due to the pressure inside the microwave reactor vessel as a result of excess reaction time. This suggests that 60 minutes could be the optimum time for synthesis of these nanostructures of Ni-Co-S using the microwave technique. For this specific period of synthesis, a steady assembly of the Ni-Co-S nano leaves into flower-like shapes was observed with no appearance of particles on the surface of the nano leaves. See figure S2-S4 in the supporting information for nano size images.

The specific surface area and porous nature of the Ni–Co–S nanomaterials produced at all concentrations and reaction times were also examined by nitrogen adsorption and desorption measurements, which are shown in Figure 3. Figure 3 revealed typical type IV isotherms for all samples with an apparent hysteresis loop, indicating a mesoporous structures with the pore size distribution inset to all the figures which demonstrates that the pores in all the samples were mesopores and macropores with a broad pore-size

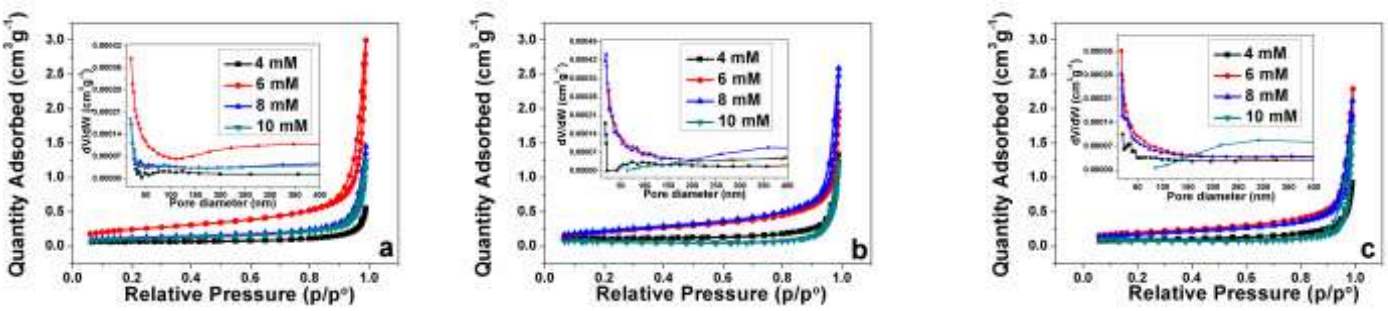

Figure 3 Nitrogen adsorption-desorption isotherm and corresponding BJH pore-size distributions (insets) of Ni-Co-S samples at different reaction times (a) 30, (b) 60 and (c) 90 minutes respectively.

distribution that ranges between 2-50 nm (inset to figure 3 (a-c)) for all the samples. The Brunauer-Emmett-Teller (BET) areas of the Ni-Co-S, sample at 30 minutes for the 4, 6, 8, 10 mM are 4.3, 12.1, 9.5, 8.1 $m^2 g^{-1}$ (figure 3a), while samples produced at 60 and 90 minutes have 7.6, 16.0, 18.1, 4.0 $m^2 g^{-1}$ and 6.6, 13.1, 15.3, 5.3 $m^2 g^{-1}$ (figure 3 b and c) respectively. From these gas sorption analysis results it is observed that the Ni-Co-S (8mM concentration of Ni+) at 60 min has a considerably higher BET values than all other produced samples. This relatively high BET values compared to other samples we attribute to complete formation of the flower like structure observed from the SEM micrographs which could lead to fast diffusion of the electrolyte as mesoporous structures can facilitate ion diffusion at the electrode-electrolyte interface during electrochemical processes. Therefore, Ni–Co–S (8 mM, 60 minutes) sample can be expected to have enhanced electrochemical performances as electrode materials. All samples with various morphology and reaction times are expected to give markedly different electrochemical properties when used as electrode for supercapacitor since the performance of an electrode is related to the materials properties. Thus, cyclic voltammetry (CV) and electrochemical impedance spectroscopy (EIS) was used to determine the best sample for Faradaic electrochemical behavior.

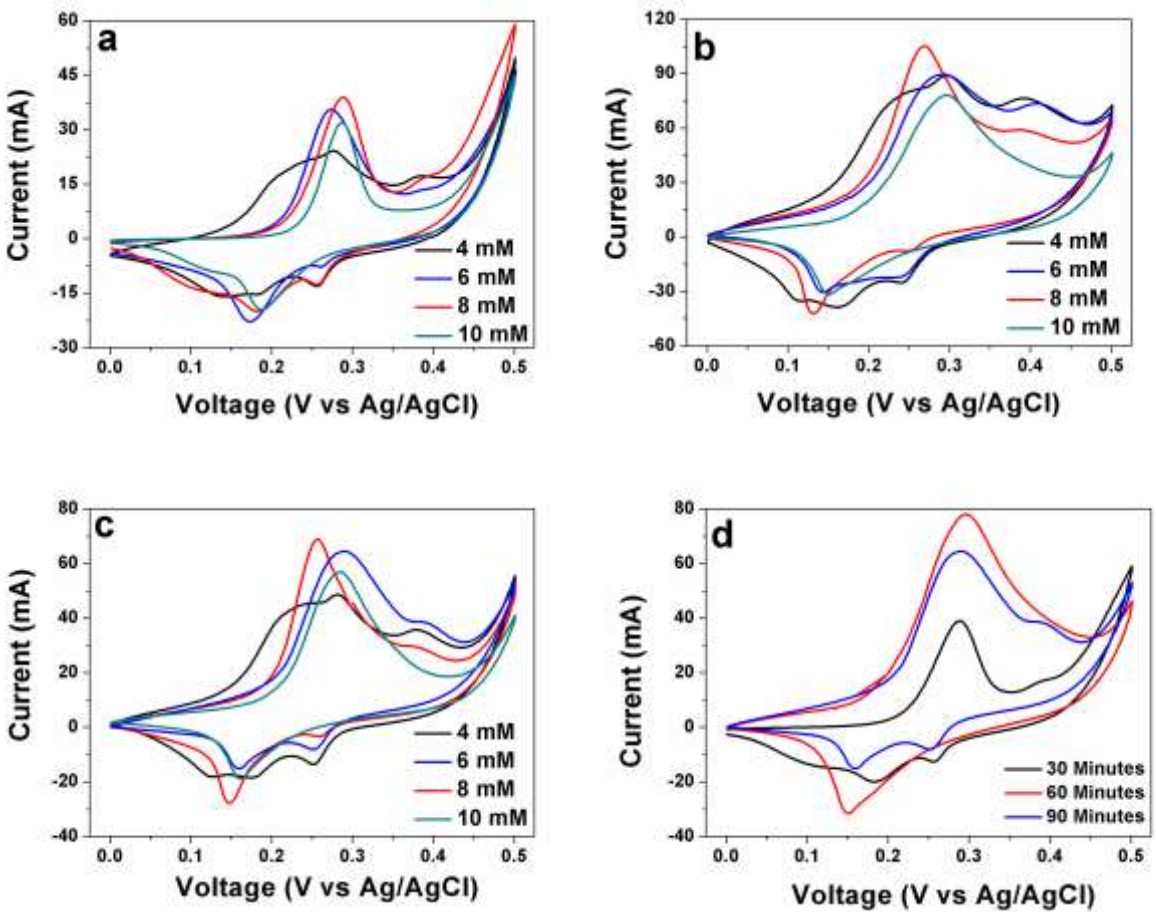

Figure 4 Cyclic voltammetry of samples produced at: (a) 30 , (b) 60, and (c) 90 minutes at a scan rate of 5 mV s^{-1} respectively and (d) CV comparison of samples with 8 mM Ni^{+} concentration produced at different reaction times at a scan rate of 5 mV s^{-1}.

Fig. 4 (a-c) shows the representative CV curves of the Ni–Co–S samples produced at different concentrations and reaction times in a potential window from 0 to 0.5 V at a scan rate of 5 mV s^{-1}. Apparently, the samples (4 6 and 8 mM) concentrations and at reaction times of 30, 60 and 90 minutes clearly show two pair of redox peaks in all their CV curves of with the exception of the 10 mM concentration at all reaction time showing just single oxidation and reduction peaks. These peaks are indication of the faradaic nature of the Ni–Co–S in the electrochemical process. The formation mechanism of these redox peaks are

probably ascribed to the reactions between the Ni–Co–S electrode materials and the alkaline electrolyte, according to the reaction below:

$$CoS + OH^- \leftrightarrow CoSOH + e^- \quad (3)$$

$$CoSOH + OH \leftrightarrow CoSO + H_2O + e^- \quad (4)$$

$$NiS + OH^- \leftrightarrow NiSOH + e^- \quad (5)$$

The first anodic peaks correspond to the oxidation of CoS to CoSOH, the second peak is the overlapped peaks of CoSOH to CoSO and NiS to NiSOH, while the two cathodic peaks represent the reverse reduction processes [30]. Also, from these CV curves, the sample with Ni of concentration 8 mM produced at 60 minutes induces a high peak current which suggest the best electrochemical response (figure 4 (d)), confirming our previous assumption that 60 minutes is the optimum growth time for such a structure in the microwave assisted hydrothermal synthesis. EIS was performed to further confirm this result and assertions.

Electrochemical impedance spectroscopy (EIS) was used to estimate the Ohmic resistance of the Ni-Co-S. Figure S5 in the supporting information shows the Nyquist plot of all the samples produced with an open-circuit potential in the frequency range of 100 kHz to 0.01 Hz. Evidently, all the curves consist of a semicircle in the high-frequency region and a straight line at the low-frequency region. The intercept on the x-axis of the Nyquist plot in the high-frequency region furnish information about the Ohmic resistance of the electrolyte and electrode material which is known as the equivalent series resistance (ESR), denoted as R_S. The semicircle is a result of charge-transfer resistance; it is denoted as R_{CT} and corresponds to the diameter of the semicircle. This vertical line in the low frequency region

indicates diffusion process taking within the structure of the material. From the EIS analysis of all the samples produced the (Ni-Co-S-3) sample grown with the following parameters (8 mM Ni^{+}, 60 minutes) showed both the least R_S (0.48 Ω) and R_{CT} (0.95 Ω). The information extracted from all the EIS spectra in figure S5 is shown in table 1. The small R_S and R_{CT} Ni-Co-S-3 are ascribed to it flower like morphology which could provide a much higher surface for

Table 1 showing all the parameter such as the R_S and the R_{CT} values obtained from the Nyquist plot fitting in figure S5.

Ni Concentration (mM)	**Reaction time (minutes)**					
	30		**60**		**90**	
	R_S (Ω)	**R_{CT} (Ω)**	**R_S (Ω)**	**R_{CT} (Ω)**	**R_S (Ω)**	**R_{CT} (Ω)**
4	0.68	1.43	0.52	2.67	0.48	1.14
6	0.65	2.43	0.50	5.11	0.56	2.36
8	0.76	1.56	**0.48**	**0.95**	0.51	1.29
10	0.50	1.12	0.52	4.11	0.55	1.04

adsorption of ion during electrochemical process and which best explain the higher rate capability by facilitating a quicker permeation process of electrolyte into the electrode matrix by shortening the diffusion distances of OH^{-} to the electroactive sites and accommodates the resulting strain caused by high rate insertion and extraction of OH−ions (figure S5 b). The EIS result also corroborates the result obtained from the CV that Ni-Co-S-3 had the best faradaic performance. Thus, all further studies are focussed on this optimized electrode.

Figure 5 (a) shows the CV curves obtained at scan rates between 5-100 mV s^{-1} for Ni-Co-S-3 sample. All CV curves exhibit a similar shape and the peak current increase with increasing

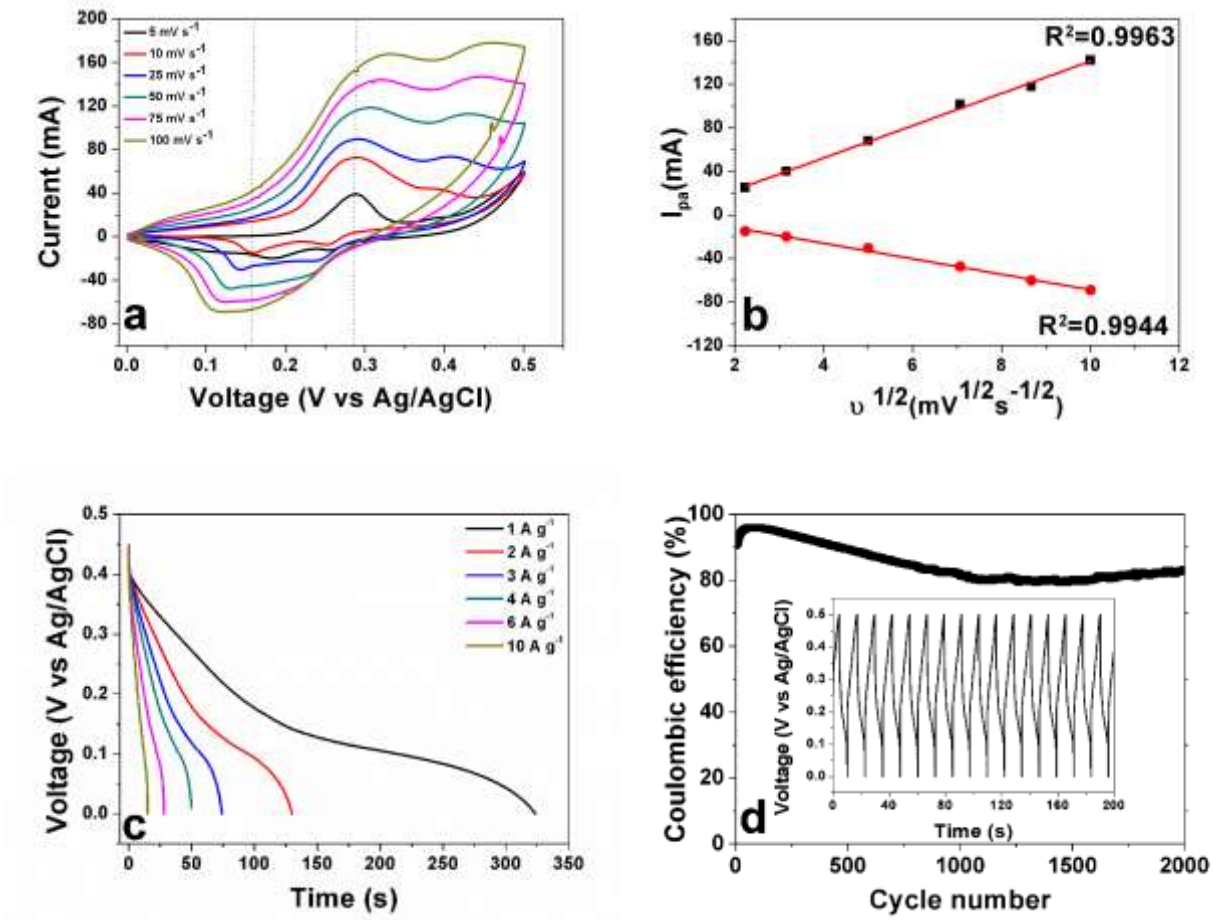

Figure 5 (a) Cyclic voltammograms of Ni-Co-S-3 sample at different scan rates (b) current (I_p) vs square root of scan rate (c) discharge curves of Ni-Co-S-3 at different current densities (d) coulombic efficiency as a function of cycle number at a current density of 5 A g^{-1}.

scan rates. Two pairs of broad redox peaks were observed corresponding to reversible faradaic pseudocapacitance electrochemical behavior of the electroactive electrodes which could be attributed to redox reaction based on Co^{2+}/Co^{3+}, Co^{3+}/Co^{4+} and Ni^{2+}/Ni^{3+} [29]. The anodic peaks shift to higher potential while the cathodic peaks shift to lower potential as the scan rate is increased probably because of kinetic in the redox process due to polarization and ohmic resistance during faradaic reactions [19,26]. Also, the shift to higher potential with increasing scan rate could be an indication of diffusion control reaction kinetics taking place during the electrochemical process. This is in line with previous

electrochemical report on cobalt sulfides and nickel sulfides which showed that cobalt sulfides showed lower redox reaction potential compared to that of nickel sulfides due to their intrinsic electrochemical response to the electrolyte [23,26]. The specific capacitance from the CV curves was estimated using equation 2. The calculated specific capacitance based on the CV curves at different scan rates of 5, 10, 25, 50, 75 and 100 mV s^{-1} were calculated to be 1110, 632, 392, 278, 225 and 190 F g^{-1} respectively. It is observed that increasing the scan rate further results in a decrease in the specific capacitance as a result of the limitation of ions within the electrode to fully access the electroactive sites at high sweep rates. The CV profiles at higher scan rates also show slight distortion which also signifies decrease in capacitance. However, the specific capacitance is still 190 F g^{-1} at a high scan rate (100 mV s^{-1}).

Figure 5 (b) shows the relationship between the scan rate and the first anodic and cathodic peak current. In this plot (Randles Servcik) a linear relationship is observed which is due to the occurrence of surface reactions and faradaic nature of the samples suggesting that the energy storage mechanism originate from the surface redox reactions of Ni^{+}. It also indicates the reaction taking place is a diffusion-controlled redox process with R^2 values being 0.9963 and 0.9944 for both anodic and cathodic processes respectively. This affirms the fast kinetics of the system which is always due to the fast rate at which electrons or ions are diffused in the materials studied. During this study, the electrode maintained stable CV when repeated at each scan rate, proving its usability in aqueous solution.

To quantify the rate capability of the Ni-Co-S-3 electrodes, galvanostatic CD measurements were carried out. Obviously, the nonlinearity in the discharge profiles (Figure 5 (c)) further verifies the electrochemical process of the Ni-Co-S-3 electrode is Faradaic in origin. Figure 5

(c) shows the discharge profiles at different current densities. The specific capacitance was calculated by using formula (1) above for the following current densities 1, 2, 3, 4, 6 and 10 A g^{-1}. The corresponding specific capacitance values of the Ni-Co-S-3 were calculated to be 790, 620, 505, 465, 330 and 347 F g^{-1} respectively. The capacitance decreases with increasing current density due to the increment of voltage drop, polarization effect and less utilization or insufficient active material during redox reaction under higher current densities [31]. These results are also consistent with the CV result which shows that the material undergoes a faradaic process.

However, at a current density of 10 A g^{-1} the sample still had a capacitance of 347 F g^{-1} suggesting a good rate capability which is very useful for the ternary sulfides electrode materials in high performance supercapacitor applications. This could be associated to the high rate capability of the bimetallic sulfides giving rise to high charge transfer conductivity which facilitates the fast transfer of electrons in the charge–discharge process. Longer cycle life is one of the most important parameters for evaluation of the electrode materials used in electrochemical processes. The coulombic efficiency which is a measure of feasibility of redox process, which is calculated from the charge-discharge curves using:

$$\eta = t_D/t_C \times 100$$

where t_C and t_D represent charging and discharging time respectively. Figure 5 (d) shows the Coulombic efficiency of the Ni-Co-S-3 as a function of the cycle number at a current density of 5 A g^{-1}. It showed relatively good electrochemical cycle stability. The specific capacitance tends to gradually decrease and then becomes stable after around 1000 cycles. As a result, there is about 80 % of the initial Coulombic efficiency after 2000 cycles, indicating the long-term cycling ability of the ternary sulfides material. Compared with other sulphide

electrodes with various morphologies in references [23-27], the capacitance values obtained in this work are quite good and comparable however the capacitance retention is moderate.

As stated earlier, EIS was used to evaluate the equivalent series resistance (ESR) or the electrical resistance responses of the Ni-Co-S-3 sulfides. Figure 6 (a) shows the Nyquist plots of the Ni-Co-S-3 sulfides before and after the last cycle were recorded in the frequency range of 0.01 Hz-100 kHz. Both plots show partial semi-circular arcs with intercept at real part representing combined resistance of electrolyte, intrinsic resistance of substrate and contact resistance at the active material/current collector. From this intercept a value of 0.48 Ω was obtained before cycling test was performed. The flower-like structure guarantees a small R_S value by providing numerous electroactive sites for Faraday reaction. In this case, facilitating a quicker permeation process of electrolyte into each the electrode matrix by shortening the diffusion distances of OH^- to the electroactive sites. However, after cycling the diffusion path length further deviates from the ideal vertical behaviour which could be attributed to the repeated cycling effect such as increment voltage drop, polarization and less utilization or insufficient active material during redox reaction during the cycling because of the high current density used. Furthermore, the diameter of semicircle for the electrode after cycle test is slightly larger after 2000 cycles, which indicates that there was an increase in the R_{CT} value which could due to the formation of inactive sites caused by the collapse of some part of flower-like structures during the cycle test. The results are good agreement with that obtained from the CD stability test that shows degradation in the Coulombic efficiency by less than 20 % after 2000 cycles.

The resulting impedance data was fitted by the Randle equivalent circuit model as shown in Figure 6 (b). In this equivalent circuit, different parameters indicated different

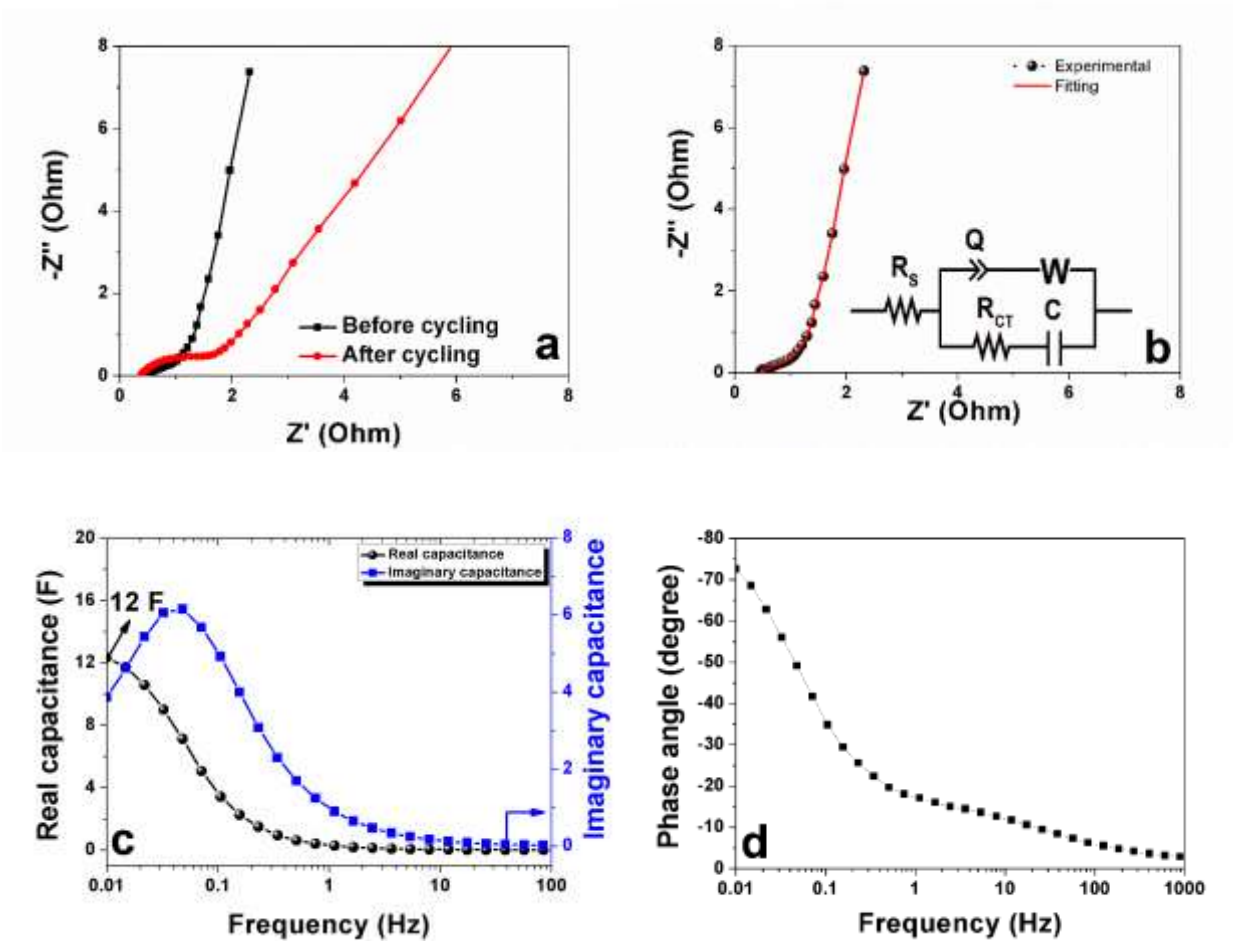

Figure 6 electrochemical impedance spectroscopy studies of Ni-Co-S-3 (a) Nyquist plot before and after cycling, (b) Nyquist fitting and circuit diagram, (c) real and imaginary capacitance as function of frequency and (d) Bode plot.

electrochemical process occurring at the electrode/electrolyte interface. From these data, several observations can be inferred from the high to the low frequency regions which correspond to different resistance phenomena during the electrochemical process. R_s is the bulk solution resistance, R_{CT} is the charge-transfer resistance, C is the capacitance, Q is the constant phase element and W is the Warburg resistance which is usually associated with leakage current. The equivalent series resistance R_S is in series with Q. The semicircle at high frequency region corresponds to the charging of the layer of Ni-Co-S-3 surface of the sample on the electrode. In the high-frequency to mid frequency region is the interfacial charge

transfer resistance R_{CT} which is in parallel with Q. The R_{CT} is caused by the interruption in the charge transfer at the electrode/electrolyte interface which is occurring between Ni-Co-S-3 and electrolyte. The R_{CT} value shown in (table 1) for Ni-Co-S-3 electrode demonstrates the collective coexistence of Ni and Co ions in the sulfides which contributes to the small value. The low charge-transfer resistance can be attributed to the high conductivity of the bimetallic sulfides [14,25]. In general, vertical line at lower frequency region indicates good capacitive behavior of the electrodes which is responsible for the ideal capacitance. The Nyquist plot shows a deviation from the vertical line in the low-frequency region indicating a near ideal capacitive behaviour and also represents the diffusion of ions at the interface between electrode and electrolyte. At these low frequencies, the current flowing through the cell usually has resistance and Warburg impedance characteristic element denoted by W which is expressed as $A/(j\omega)^{0.5}$ where A is the Warburg coefficient, ω is the angular frequency. In the Nyquist plots the inclined portion of the curve at lower frequency near 45 is attributed to the Warburg impedance, W, which is caused by the diffusion/transport of OH^- ions within the pores or surface of Ni-Co-S-3 electrodes during the redox reactions.

Table 2 Fitting parameters for the Ni-Co-S-3 electrode.

R_S (Ω)	**Q ($F.s^{(a-1)}$)**	**R_{CT} (Ω)**	**C (F)**	**n**	**A_W ($Ω.s^{-.5}$)**
0.47	**2.33**	**1.05**	**1.086**	**1**	**1.422**

X^2 = 0.0588, $X/\sqrt{N}$ = 0.037.

Table 2 above presents the R_S, R_{CT} values and other parameters used for fitting without any further adjustments which indicates an optimized minimization of experimental data and design of the Ni-Co-S-3 electrode material with an error of 0.037. X^2 represents the criterion

for minimization of the fit. $X/\sqrt{N}$ with N being the number of points, is a normalized expression of X^2, whose value is independent of number of points and represented the error above. The frequency response of the electrodes modelled with a single series resistor-capacitor (RC) circuit is shown in figure 6 (c) the real part of the capacitance can be calculated using the equation below

$$C = -1/\omega Z''$$

where Z" is the imaginary part of the impedance and ω is the frequency. Based on the above formulae the real or deliverable capacitance as a function of frequency specific capacitance has been calculated to be 12 F (intercept on the vertical axis of figure 6 (c). The imaginary capacitance is used to estimate the time constant. The characteristic frequency (f_0) which corresponds to peak of imaginary capacitance is used. From this a corresponding time constant $\tau = 1/f_0 = 25\,\mathrm{s}$ was estimated. The dependence of phase angle on the frequency for the Ni-Co-S-3 electrode is shown in figure 6 (d) and shows that the phase angle of -73° close to 90° at low frequencies which confirms a nearly ideal capacitive behaviour.

Due to the fact that our Ni-Co-S-3 sample showed exceptional properties as stated above we decided to check its magnetic properties. The low field magnetization of this sample as function of temperature from 4 K to 300 K is shown in figure 7 (a) with the inset to the figure being the enhanced section of low temperature range. There is a clear peak at 10 K which corresponds to transition temperature below which this material is ferromagnetic. To further test the magnetic property of this material, field dependent magnetization below and above transition temperature was carried out. Figure 7 (b), (c) and (d) show magnetization as function of external field being circled back and forth at 5, 20 K and 300 K respectively. An s-shape like magnetization curve showing saturation at 2 T with no

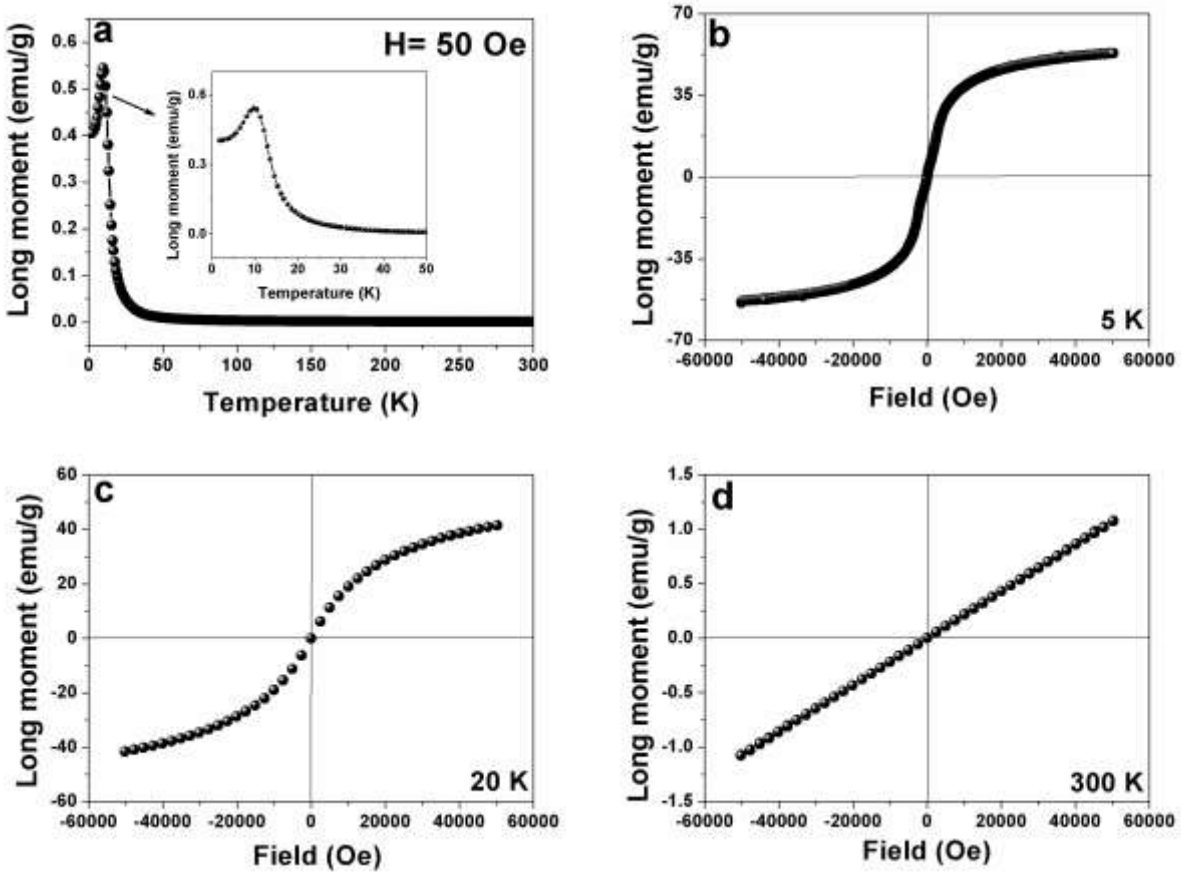

Figure 7 Magnetization measurements of Ni-Co-S-3 (a) temperature dependence at 50 Oe (inset to the figure represent low temperature region of the main figure), (b), (c) and (d) applied field dependent at 5 K, 20K and 300 K respectively.

hysteresis at 5 K is a clear indication that this nano-structured material with particle size ranging between 25 – 30 nm, exhibits magnetic behaviour at this temperature. Above 10 K the magnetization starts to be linear with temperature with no hysteresis loop observed either. This nano-sized magnetic material with grain-sized single domain magnetic moments, which has no hysteresis at any temperature is said to be superparamagnetic. The detailed study of the origin of magnetism in this material is still underway.

Conclusion

In summary, we have successfully synthesized flower-like nanosheets of $Ni_xCo_yS_4$ with different Ni and Co content and optimum time by a microwave method. The bimetallic

composition with the 2:1 (Ni-Co-S) stoichiometry showed the best electrochemical results in terms of specific capacitance, good rate capability and long cycle stability. Overall, the ternary Ni-Co-S-3 sample showed good electrochemical activity due it bimetallic conductivity, rich redox reactions involving different ions and their synergetic effects. These results demonstrate that high performance supercapacitive materials can be engineered through optimization of the stoichiometric properties by tuning the content properties of bimetallic component. Furthermore, the materials showed super-paramagnetic behaviour demonstrating that they are truly nano-sized with grain-sized single domain moments.

Acknowledgement

This work is based upon research supported by the South African Research Chairs Initiative of the South African Department of Science and Technology (SARCHi-DST) and the National Research Foundation (NRF). Any opinion, findings and conclusions or recommendations expressed in this work are those of authors and therefore the NRF and DST do not accept any liability with regard thereto. AB, and OOF, acknowledges University of Pretoria and NRF financial support for Postdoc fellowship, while DYM, FB, MJM and TMM acknowledge financial support from University of Pretoria and the NRF for PhD bursaries.

References

[1] A.S. Aricò, P. Bruce, B. Scrosati, J.-M. Tarascon, W. Van Schalkwijk, Nanostructured materials for advanced energy conversion and storage devices, Nat. Mater. 4 (2005) 366–377.

[2] B. Dunn, H. Kamath, J.-M. Tarascon, Electrical energy storage for the grid: a battery of choices., Science. 334 (2011) 928–35.

[3] P. Simon, Y. Gogotsi, Materials for electrochemical capacitors, Nat. Mater. 7 (2008) 845–854.

[4] A.K. Mondal, D. Su, S. Chen, K. Kretschmer, X. Xie, H.-J. Ahn, G. Wang, A Microwave Synthesis of Mesoporous NiCo2O4 Nanosheets as Electrode Materials for Lithium-Ion Batteries and Supercapacitors, ChemPhysChem. 16 (2015) 169–175.

[5] B. Saravanakumar, K.K. Purushothaman, G. Muralidharan, Interconnected V_2O_5 nanoporous network for high-performance supercapacitors, ACS Appl. Mater. Interfaces. 4 (2012) 4484–4490.

[6] Z. Cui, W. Yuan, C.M. Li, Template-mediated growth of microsphere, microbelt and nanorod α-MoO_3 structures and their high pseudo-capacitances, J. Mater. Chem. A. 1 (2013) 12926–12931.

[7] P.J. Hall, M. Mirzaeian, S.I. Fletcher, F.B. Sillars, A.J.R. Rennie, G.O. Shitta-Bey, G. Wilson, A. Cruden, R. Carter, Energy storage in electrochemical capacitors: designing functional materials to improve performance, Energy Environ. Sci. 3 (2010) 1238–1251.

[8] J. Jiang, Y. Li, J. Liu, X. Huang, C. Yuan, X.W.D. Lou, Recent Advances in Metal Oxide-based Electrode Architecture Design for Electrochemical Energy Storage, Adv. Mater. 24 (2012) 5166–5180.

[9] R.B. Rakhi, W. Chen, D. Cha, H.N. Alshareef, Substrate dependent self-organization of mesoporous cobalt oxide nanowires with remarkable pseudocapacitance., Nano Lett. 12 (2012) 2559–67.

[10] C.O. Kappe, D. Dallinger, Controlled microwave heating in modern organic synthesis: highlights from the 2004--2008 literature, Mol. Divers. 13 (2009) 71–193.

[11] A. Bello, O.O. Fashedemi, M. Fabiane, J.N. Lekitima, K.I. Ozoemena, N. Manyala, Microwave assisted synthesis of MnO 2 on nickel foam-graphene for electrochemical capacitor, Electrochim. Acta. 114 (2013) 48–53.

[12] W. Wei, X. Cui, W. Chen, D.G. Ivey, Manganese oxide-based materials as electrochemical supercapacitor electrodes., Chem. Soc. Rev. 40 (2011) 1697–721.

[13] S.-W. Chou, J.-Y. Lin, Cathodic deposition of flaky nickel sulfide nanostructure as an electroactive material for high-performance supercapacitors, J. Electrochem. Soc. 160 (2013) D178–D182.

[14] J. Xiao, L. Wan, S. Yang, F. Xiao, S. Wang, Design hierarchical electrodes with highly conductive $NiCo_2S_4$ nanotube arrays grown on carbon fiber paper for high-performance pseudocapacitors, Nano Lett. 14 (2014) 831–838.

[15] X. Xia, C. Zhu, J. Luo, Z. Zeng, C. Guan, C. F. Ng, H Zhang, H. J. Fan Synthesis of Free-Standing Metal Sulfide Nanoarrays via Anion Exchange Reaction and Their Electrochemical Energy Storage Application, Small. 10 (2014) 766–773.

[16] Z. Bai, N. Fan, C. Sun, Z. Ju, C. Guo, J. Yang, Y. Qian, Facile synthesis of loaf-like $ZnMn_2O_4$ nanorods and their excellent performance in Li-ion batteries, Nanoscale. 5 (2013) 2442–2447.

[17] C. Fu, G. Li, D. Luo, X. Huang, J. Zheng, L. Li, One-Step Calcination-Free Synthesis of Multicomponent Spinel Assembled Microspheres for High-Performance Anodes of Li-Ion Batteries: A Case Study of $MnCo_2O_4$, ACS Appl. Mater. Interfaces. 6 (2014) 2439–2449.

[18] C. Yuan, H. Bin Wu, Y. Xie, X.W.D. Lou, Mixed Transition-Metal Oxides: Design, Synthesis, and Energy-Related Applications, Angew. Chemie Int. Ed. 53 (2014) 1488–1504.

[19] E. Umeshbabu, G. Rajeshkhanna, G.R. Rao, Urchin and sheaf-like $NiCo_2O_4$ nanostructures: Synthesis and electrochemical energy storage application, Int. J. Hydrogen Energy. 39 (2014) 15627–15638.

[20] Y. Liu, J. Zhang, S. Wang, K. Wang, Z. Chen, Q. Xu, Facilely constructing 3D porous $NiCo_2S_4$ nanonetworks for high-performance supercapacitors, New J. Chem. 38 (2014) 4045–4048.

[21] J. Pu, T. Wang, H. Wang, Y. Tong, C. Lu, W. Kong, et al., Direct Growth of $NiCo_2S_4$ Nanotube Arrays on Nickel Foam as High-Performance Binder-Free Electrodes for Supercapacitors, Chempluschem. 79 (2014) 577–583.

[22] J. Pu, F. Cui, S. Chu, T. Wang, E. Sheng, Z. Wang, Preparation and Electrochemical Characterization of Hollow Hexagonal NiCo2S4 Nanoplates as Pseudocapacitor Materials, ACS Sustain. Chem. Eng. 2 (2013) 809–815.

[23] L. Yu, L. Zhang, H. Bin Wu, X.W.D. Lou, Formation of $NixCo_{3-x}S_4$ Hollow Nanoprisms with Enhanced Pseudocapacitive Properties, Angew. Chemie. 126 (2014) 3785–3788.

[24] H. Chen, J. Jiang; L. Zhang, D. Xia, Y. Zhao, D. Guo, T. Qi, H. Wan, In situ growth of NiCo 2 S 4 nanotube arrays on Ni foam for supercapacitors: Maximizing utilization efficiency at high mass loading to achieve ultrahigh areal pseudocapacitance, J. Power Sources. 254 (2014) 249–257.

[25] H. Chen, J. Jiang, L. Zhang, H. Wan, T. Qi, D. Xia, Highly conductive $NiCo_2S_4$ urchin-like nanostructures for high-rate pseudocapacitors, Nanoscale. 5 (2013) 8879–8883.

[26] W. Chen, C. Xia, H.N. Alshareef, One-Step Electrodeposited Nickel Cobalt Sulfide Nanosheet Arrays for High-Performance Asymmetric Supercapacitors, ACS Nano. 8 (2014) 9531–9541.

[27] H. Chen, J. Jiang, Y. Zhao, L. Zhang, D. Guo, D. Xia, One-pot synthesis of porous nickel cobalt sulphides: tuning the composition for superior pseudocapacitance, J. Mater. Chem. A. 3 (2015) 428–437.

[28] C.O. Kappe, How to measure reaction temperature in microwave-heated transformations., Chem. Soc. Rev. 42 (2013) 4977–90.

[29] L. Zhang, H. B. Wua, X. W. (David) Lou Unusual CoS_2 ellipsoids with anisotropic tube-like cavities and their application in supercapacitors, Chem. Commun. 48 (2012) 6912–6914.

[30] H. Wan, J. Jiang, J. Yu, K. Xu, L. Miao, L. Zhang, H. Chen, Y. Ruan, $NiCo_2S_4$ porous nanotubes synthesis via sacrificial templates: high-performance electrode materials of supercapacitors, CrystEngComm. 15 (2013) 7649–7651.

[31] S. Xiong, C. Yuan, X. Zhang, Y. Qian, Mesoporous NiO with various hierarchical nanostructures by quasi-nanotubes/nanowires/nanorods self-assembly: controllable preparation and application in supercapacitors, CrystEngComm. 13 (2011) 626–632.

Supporting Information

a) 30 minutes

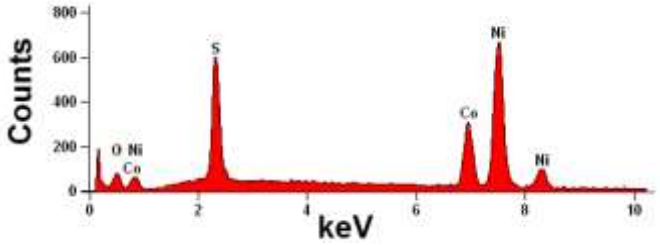

b) 60 minutes

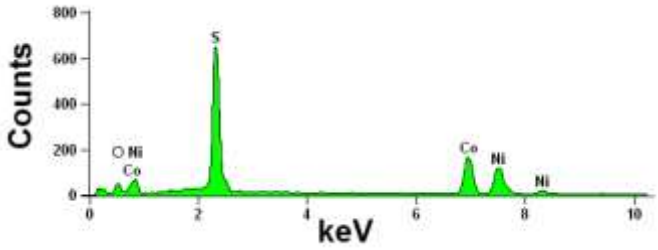

c) 90 minutes

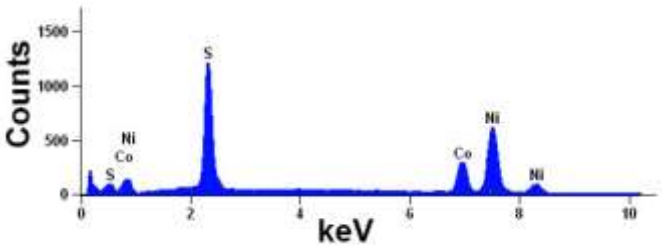

Figure S1. EDX pattern of the representative Ni-Co-S produced at different times of (a) 30, (b) 60 and (c) 90 minutes respectively.

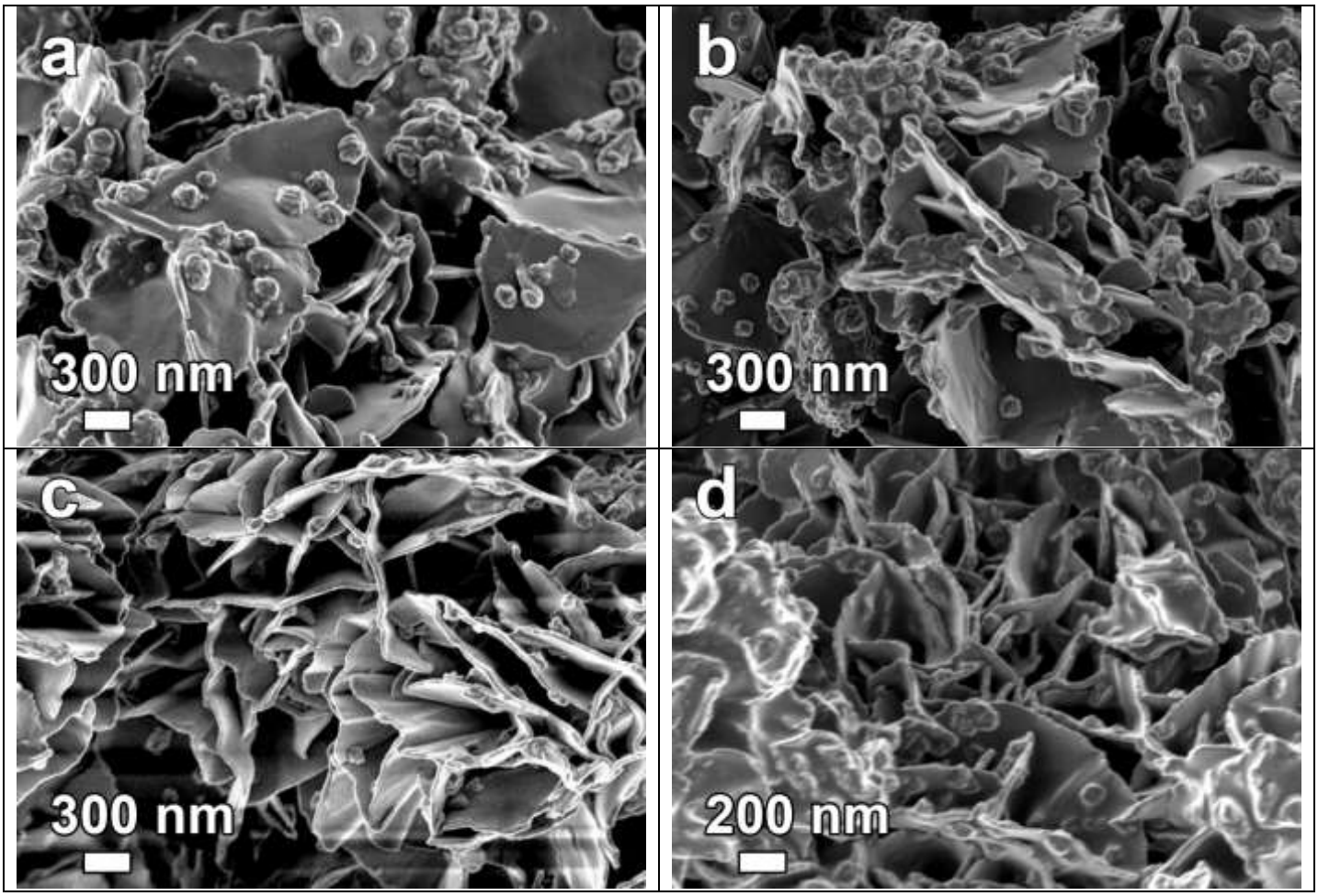

Figure S2 High magnification SEM micrographs of Ni-Co-S produced at 30 minutes with different concentration of Ni^{+} ion: (a) 4 mM, (b) 6 mM, (c) 8 mM, and (d) 10 mM .

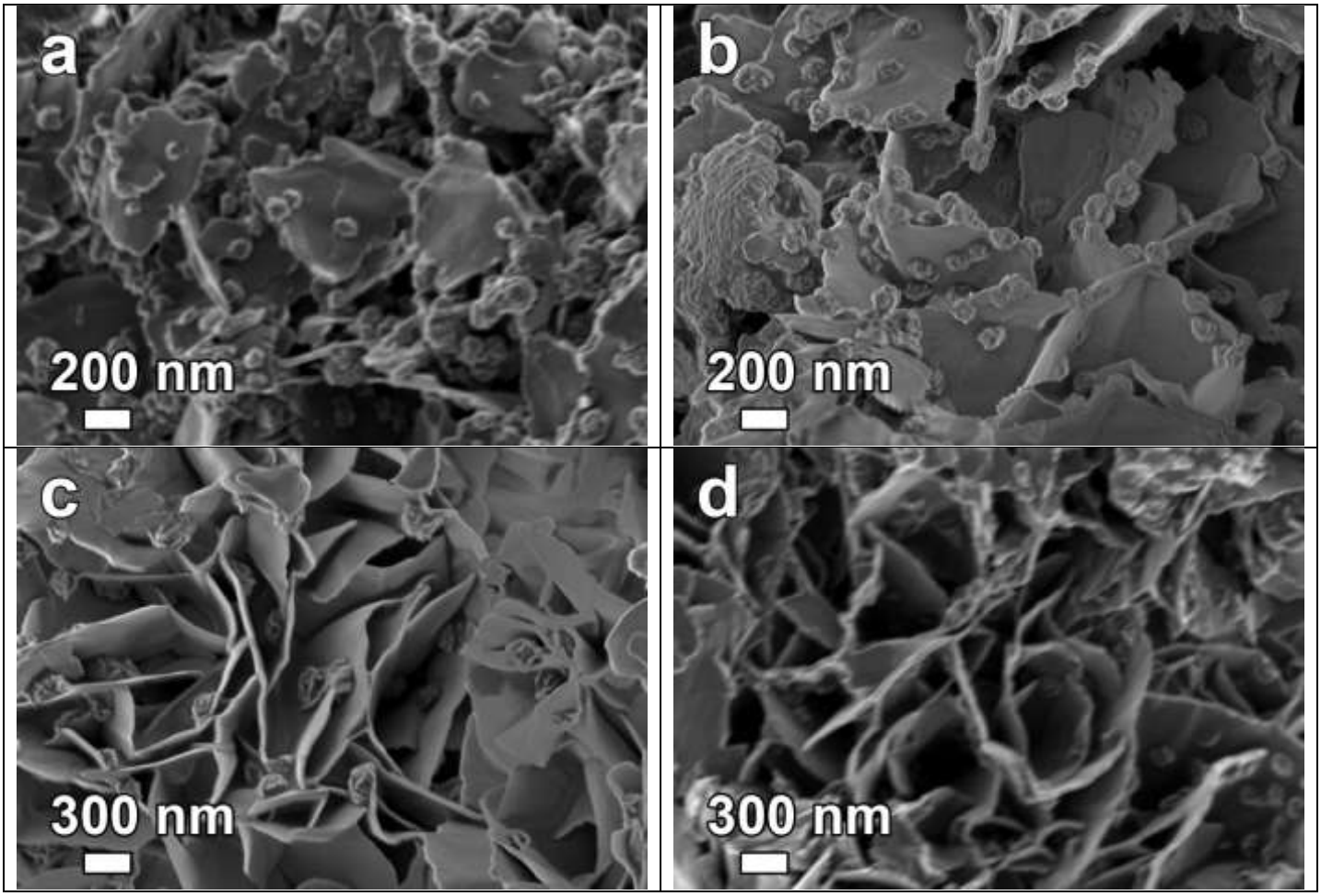

Figure S3 High magnification SEM micrographs of Ni-Co-S produced at 60 minutes with different concentration of Ni^{+} ion: (a) 4 mM, (b) 6 mM (c) 8 mM and (d) 10 mM .

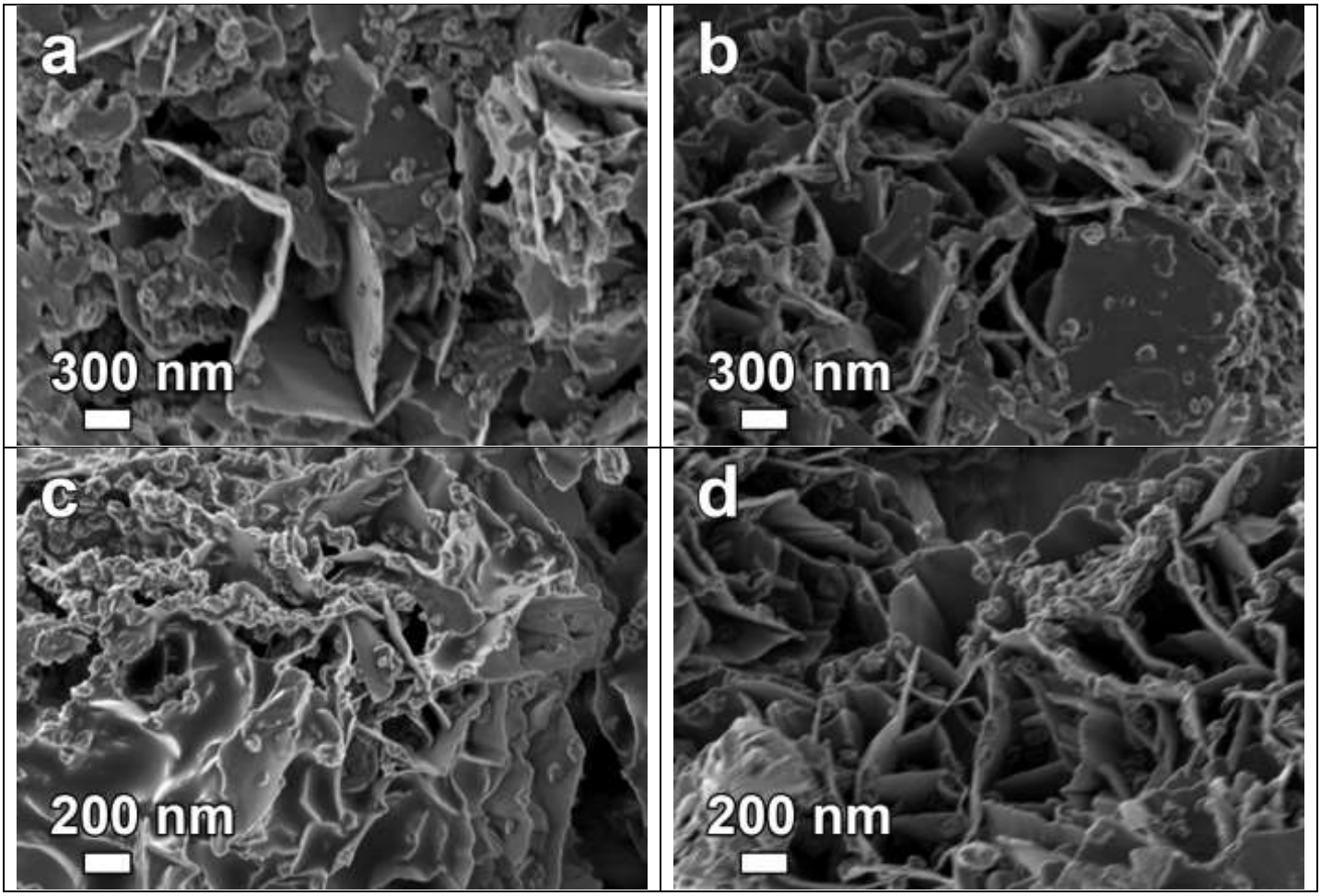

Figure S4 High magnification SEM micrographs of Ni-Co-S produced at 90 minutes with different concentration of Ni^{+} ion: (a) 4 mM, (b) 6 mM (c) 8 mM and (d) 10 mM .

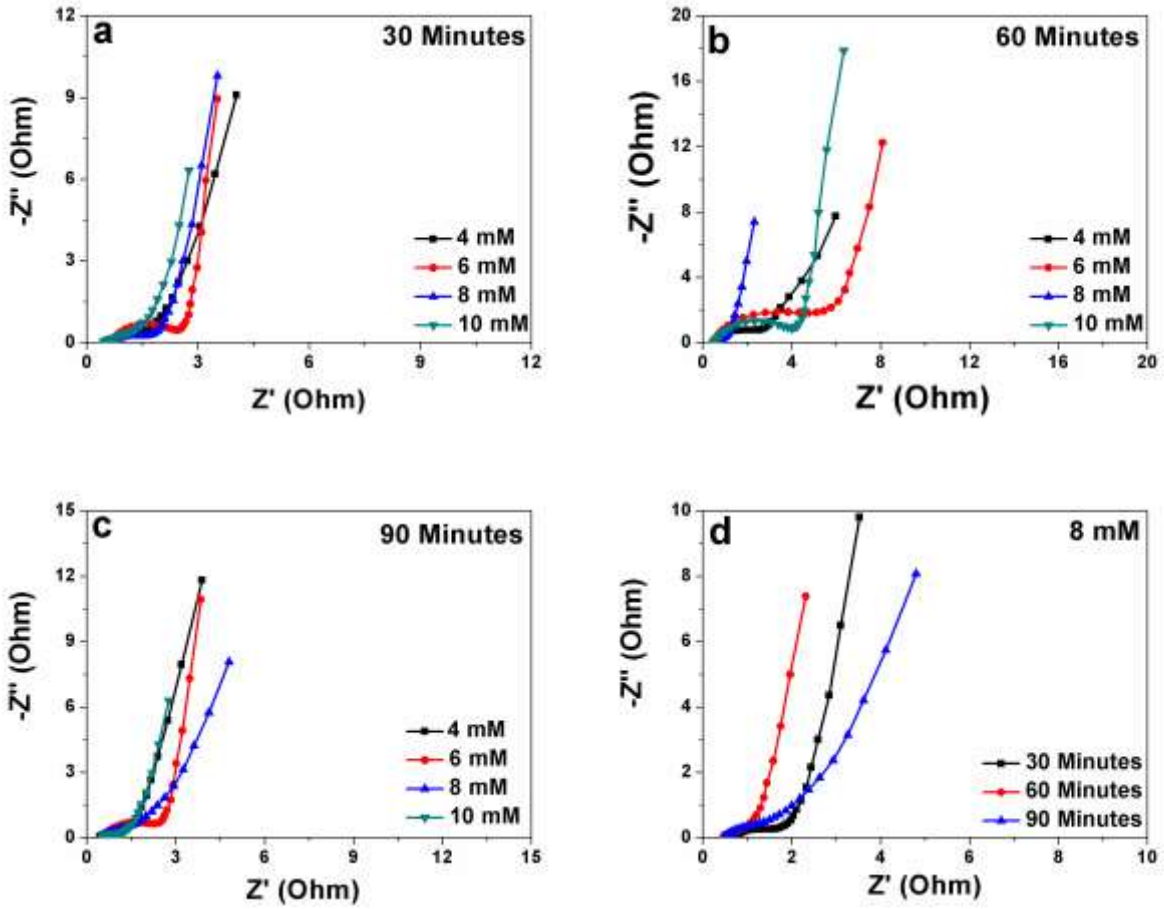

Figure S5 Nyquist plots of (a) 30, (b) 60, (c) 90 minutes samples respectively, and (d) compares samples at different reaction times.